01 Sep 2012

Stochastic Simulation of Entangled Polymeric Liquids in Fast Flows: Microstructure Modification

Joontaek Park
Missouri University of Science and Technology, parkjoon@mst.edu

David W. Mead

Morton M. Denn

Recommended Citation

J. Park et al., "Stochastic Simulation of Entangled Polymeric Liquids in Fast Flows: Microstructure Modification," *Journal of Rheology*, vol. 56, no. 5, pp. 1057-1081, American Institute of Physics (AIP), Sep 2012.
The definitive version is available at https://doi.org/10.1122/1.4720086

Stochastic simulation of entangled polymeric liquids in fast flows: Microstructure modification

Article *in* Journal of Rheology · September 2012
DOI: 10.1122/1.4720086

3 authors, including:

Joontaek Park
Missouri University of Science and Technology
33 PUBLICATIONS **100** CITATIONS
SEE PROFILE

Morton Denn
City College of New York
251 PUBLICATIONS **7,189** CITATIONS
SEE PROFILE

Stochastic simulation of entangled polymeric liquids in fast flows: Microstructure modification

Joontaek Park, David W. Mead, and Morton M. Denn[a)]

Benjamin Levich Institute and Department of Chemical Engineering, The City College of New York, CUNY, New York, New York 10031

(Received 24 June 2011; final revision received 30 April 2012; published 19 June 2012)

Synopsis

We have modified the full-chain stochastic tube (XDS) model developed by Xu *et al*. [J. Rheol. **50**, 477–494 (2006)] to simulate the rheology of entangled melts and solutions of linear monodisperse polymers. The XDS model, which has a single adjustable parameter that is equivalent to the Rouse time, successfully describes steady and transient shear and normal stress data at low to moderate rates, but the results deviate systematically from experimental data at high rates. The algorithm for re-entanglement was revised, and a configuration-dependent friction coefficient (CDFC), as originally proposed by Giesekus, was incorporated to account for microstructural change of the tube away from equilibrium. The simulation results from the modified model significantly reduce the deviation from the experimental data in shear, and they also agree well with extensional data for entangled solutions, including an initial −0.5-power dependence of the steady extensional viscosity on extension rate. We also applied the CDFC to the molecular model developed by Mead *et al*. [Macromolecules **31**, 7895–7914 (1998)] and obtained improved predictive performance at high deformation rates, reinforcing the idea that there is a structural change in the tube far from equilibrium that accelerates relaxation processes. Finally, noting that molecular models make fundamentally different assumptions about the effect of the deformation on the entanglement density but give essentially equivalent rheological predictions, we explored the effect of the dynamics of the entanglement density by changing the entanglement assumptions in the stochastic model. © *2012 The Society of Rheology*. [http://dx.doi.org/10.1122/1.4720086]

I. INTRODUCTION

The tube model [Doi and Edwards (1986)], first postulated by Edwards (1967) and subsequently refined by many authors, quantitatively simulates linear and moderately nonlinear flows of monodisperse and polydisperse linear and branched entangled polymer melts and solutions [McLeish (2002)].

The tube concept as originally formulated is an equilibrium construct. Numerous modifications [for example, Doi (1983); Pearson *et al*. (1991); Ianniruberto and Marrucci (1996); Mead *et al*. (1998); McLeish (2002)] have been made to the original tube model to improve the prediction of rheological behavior near equilibrium and in weak flows, predicated on the assumption of a constant equilibrium tube structure. Graham *et al*. (2003) claimed that the entanglement microstructure of the tube is effectively the

[a)]Author to whom correspondence should be addressed; electronic mail: denn@ccny.cuny.edu

equilibrium microstructure as long as $\dot{\gamma}\tau_e \ll 1$, where $\dot{\gamma}$ is a shear rate and τ_e denotes the Rouse (equilibration) time of a single tube segment. When the chain segments become highly aligned, however, the microstructure of the tube is unlikely to be that of the equilibrium state, and the proper formulation for nonlinear simulations within the framework of the tube model is not yet firmly established. We focus on the highly nonlinear rheological properties in this manuscript. In particular, we demonstrate that systematic departures of tube model predictions from experimental data at high deformation rates suggest that changes in the entanglement microstructure defining the tube may be occurring. This observation is supported by experimental evidence of "rupture" of entangled polymers in well defined uniaxial extension experiments at high stress levels [Joshi and Denn (2004a, 2004b); Burghelea *et al.* (2009)]. Since most polymer processing operations operate in the highly nonlinear regime [e.g., Denn (2008)], resolving the outstanding issues in this flow regime is highly relevant.

It is well known that new physical phenomena manifest themselves in entangled polymers under conditions that go beyond the original construct, and modifications to the basic tube model to describe these phenomena have progressed according to the classic methodology of the scientific method by first identifying a systematic deviation of tube model predictions from experimental data and then introducing new physical concepts that are compatible with the basic construct where it applies. This is the process whereby such modifications as dynamic dilution in star polymer rheology [Ball and McLeish (1989)], convective constraint release [Marrucci (1996); Ianniruberto and Marrucci (1996); Mead *et al.* (1998)], Rouse-like motion of the tube in star-linear blends [Milner *et al.* (1998)], component stretch in fast extensional flows of polydisperse systems [Auhl *et al.* (2009)], and tube dilation [Struglinski and Graessley (1988)] have been made. Convective constraint release, in particular, is an entirely nonlinear flow effect that introduces the notion of a dynamic tube in fast flows. In this work, we consider another fully nonlinear effect on the molecular rheology of monodisperse entangled polymers, namely, a configuration-dependent friction coefficient (CDFC).

Stochastic simulators have proven to be effective research tools for probing new physical phenomena in entangled polymers in a way that is free of the inherent compromises and ambiguities associated with closed-form analytical constitutive models that contain physical and analytical approximations [e.g., the MLD model of Mead *et al.* (1998) and the GLaMM model of Graham *et al.* (2003)] and with less computational load but clearer morphological information than associated with molecular dynamics simulations, such as those by Kremer and Grest (1990), Everaers *et al.* (2004), and Likhtman *et al.* (2007). Stochastic models for entangled polymeric liquids generally consist of two dynamic components: (1) Brownian dynamics of a polymer chain along its primitive path in tubelike topological constraints [de Gennes (1971)] and (2) dynamics of the confining tubes that are affinely deformed by flows. Instead of simulating the virtual tubes directly, the proper choice of a mean field model for the constraints can reduce complexity without losing the key dynamics.

Based on the way in which the virtual tube is represented, the stochastic models can be separated according to three approaches: point obstacles, slip-links, and an axisymmetric mean field harmonic potential. The "repton" model by Rubinstein (1987) discretized the tube by point obstacles. The original idea of the slip-link [Doi and Edwards (1978a, 1978b, 1978c, 1979), Edwards and Vilgis (1986)] was further developed by Öttinger (1999), Fang *et al.* (2000), Gigras and Khomami (2002), Greco (2002), Rubinstein and Panyukov (2002), Likhtman (2005), Tasaki *et al.* (2001), and Doi and Takimoto (2003). A "full-chain model" [Hua and Schieber (1998); Hua *et al.* (1998, 1999); Neergaard *et al.* (2000)] was later developed into a consistently unconstrained Brownian slip-link (CUBS) model [Nair and Schieber (2006); Schieber *et al.* (2007)]. The multichain

primitive chain network (PCN) slip-link model of Masubuchi *et al.* (2001, 2003) was further modified [Yaoita *et al.* (2008)] and recently adapted by Dambal *et al.* (2009) and Kushwaha and Shaqfeh (2011).

The "stochastic tube model," which is our initial focus here, represents the tubelike confinement as an axisymmetric mean field harmonic potential. The topological restraints in this model are very similar to the original virtual tube concept by de Gennes (1971). Xu *et al.* (2006) developed this tube model by incorporating the harmonic potential into the full-chain model [Hua and Schieber (1998); Hua *et al.* (1998, 1999)]. A harmonic potential in the form of a transverse force regulates polymer chain departures from the tube axis. The transverse force was derived self-consistently, so that it maintains the equilibrium tube contour length and diameter in the absence of flow. The model by Xu *et al.* (2006) effectively removed several limitations of the full-chain model [Hua and Schieber (1998); Hua *et al.* (1998, 1999)]: specifically, (1) chain loop formation within a tube is possible, as in the repton model [Rubinstein (1987)]; (2) the constraint release/creation kinetics are self-consistent; and (3) the computed stress is independent of the number of beads in the simulation. This stochastic simulator, which has only a single adjustable parameter defining the time scale, successfully predicted the rheological behavior of entangled polymers at low to moderate shear rates [Xu *et al.* (2006)] and was also applied to the study of apparent wall slip [Xu *et al.* (2007)].

The stochastic models mentioned above have shown reasonable agreement with experimental data, but not all of the phenomena and conditions are satisfied according to each model's characteristic assumptions and approximations. For example, Ye *et al.* (2003) adjusted the chain extensibility parameter in the MLD model of Mead *et al.* (1998) to fit extensional flow data at high strain rates. The CUBS model by Schieber *et al.* (2007) showed anomalously oscillating behavior in transient extensional stress, making it difficult to get a reliable steady extensional viscosity. When the stochastic tube model of Xu *et al.* (2006) was applied to higher shear rates and extensional flows, systematic deviation from the experimental data caused by excessive stretch occurred, as will be shown in later sections.

In this work, we propose modifications to the full-chain stochastic tube model of Xu *et al.* (2006), hereafter denoted as XDS, so that the revised model, denoted as PMD, can be applied to very high deformation rates and extensional flows. We interrogated the re-entanglement process and found that a revision is required at higher deformation rates that conserves the total contour length of tubes in the ensemble during constraint release and creation. We conjecture that the tube structure may result in reduced friction for highly aligned configurations. Thus, the two modifications we implement are as follows: (1) the preservation of the total contour length of the tube in an ensemble during the re-entanglement process and (2) the incorporation of a configuration-dependent friction coefficient, which depends on the relative alignment of segments with the matrix chains.

The paper is organized as follows: Sec. II describes the previous XDS model, as well as the modifications implemented for this study (PMD model). In Sec. III, the systematic deviation of the XDS simulator in predicting rheological experimental data at high shear rates is shown, followed by the demonstration of the dramatic reduction in deviation by the PMD model. The results from the application of the revised model to extensional flows are also shown. Section IV shows the confirmation of the CDFC concept at high deformation rates. We also apply the CDFC concept here to the MLD molecular model. Conclusions are drawn in Sec. V. Additionally, we have investigated the microstructural change in terms of the entanglement dynamics during the re-entanglement process, and some preliminary results are described in the Appendix.

II. MODEL DESCRIPTION

A. Governing equations

The full-chain stochastic tube model simulates entangled polymer chains as an ensemble of N_C individual bead-spring chains within tubes. Figure 1 shows a schematic diagram of how the model represents an entangled polymer chain. The polymer chain consists of N beads and N–1 springs. The Z virtual tube segments confine the polymer chain by two forces: a transverse force, $\mathbf{F}^R$, which restrains the chain in the direction normal to the tube axis, and a tensile force, $\mathbf{F}^T$, which acts along the chain to maintain the primitive path as a random walk. The ith bead position is denoted as $\mathbf{R}_i$, and the primitive path vector of the zth tube segment is represented by $\mathbf{U}_z$; the corresponding unit vector $\mathbf{u}_z = \mathbf{U}_z/|\mathbf{U}_z|$. The dynamics of an unconstrained polymer chain are described by the spring force, $\mathbf{F}^S$; the Brownian force, $\mathbf{F}^B$; and the viscous drag. Inertia is neglected. The governing equation for the entangled polymer chain can therefore be expressed as a series of coupled Langevin equations for each of the N beads, including the two confining forces:

$$\begin{aligned} 0 &= -\zeta_1\left[\dot{\mathbf{R}}_1 - \kappa\cdot\mathbf{R}_1\right] + \mathbf{F}_1^S + \mathbf{F}_1^R - \mathbf{F}_1^T + \mathbf{F}_1^B, \\ 0 &= -\zeta_i\left[\dot{\mathbf{R}}_i - \kappa\cdot\mathbf{R}_i\right] + \mathbf{F}_i^S - \mathbf{F}_{i-1}^S + \mathbf{F}_i^R + \mathbf{F}_i^B, \quad 2 \le i \le N-1, \\ 0 &= -\zeta_N\left[\dot{\mathbf{R}}_N - \kappa\cdot\mathbf{R}_N\right] - \mathbf{F}_{N-1}^S + \mathbf{F}_N^R + \mathbf{F}_N^T + \mathbf{F}_N^B. \end{aligned} \tag{1}$$

Here, ζ_i is a friction coefficient, which is taken to be the same for all beads in the original XDS model but may be dependent on relative segment/matrix configuration in our formulation here. The velocity gradient tensor is denoted as $\boldsymbol{\kappa}$.

The spring force between beads is described by the nonlinear FENE model

$$\mathbf{F}_i^S = \frac{H(\mathbf{R}_{i+1} - \mathbf{R}_i)}{1 - (\mathbf{R}_{i+1} - \mathbf{R}_i)^2/b^2}. \tag{2}$$

Here, H and b are the linear spring constant and the maximum extensibility of the spring, which are, respectively,

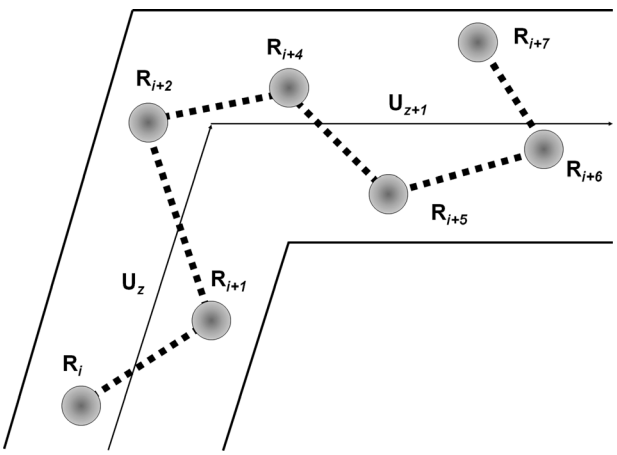

FIG. 1. Sketch of a part of the chain confined within two consecutive tube segments.

$$H = \frac{3k_BT(N-1)}{N_K a_K^2} \quad \text{and} \quad b = \frac{N_K a_K}{(N-1)}, \tag{3}$$

where a_K is the Kuhn length and N_K is the number of Kuhn steps in a chain.

The Brownian forces are derived from the fluctuation-dissipation theorem and can be expressed in a discretized form for a numerical time step Δt using a random vector $\mathbf{w}_i$ that has a unit variance and zero mean [e.g., Van Kampen (1992)]:

$$\mathbf{F}_i^B = \sqrt{\frac{2k_BT\zeta_i}{\Delta t}}\mathbf{w}_i. \tag{4}$$

The tensile force, which follows the distribution function for a flexible polymer chain confined in a tube [Doi and Edwards (1986)], is given as

$$\mathbf{F}_i^T = \frac{3k_BT}{\sqrt{\frac{N_K a_K^2}{Z_{eq}}}}\,\mathbf{u}_z = \frac{3k_BT}{L_{eq}}\mathbf{u}_z. \tag{5}$$

Here, Z_{eq} is the average number of entanglements at equilibrium and L_{eq} is the average equilibrium length of an entangled chain segment.

The transverse force was derived self-consistently by Xu *et al.* (2006) to ensure that each chain is confined in an axisymmetric harmonic potential well and maintains the equilibrium contour length of each tube at L_{eq}:

$$\mathbf{F}_i^R = -\alpha_i \mathbf{P}_i, \tag{6}$$

$$\alpha_i = \begin{cases} -\frac{2(K-1)}{K}H & i = 1, N \\ \left(-4 - \frac{2}{K-2} + \frac{2}{K}\right)H & i \neq 1, N \end{cases}. \tag{7}$$

Here, $\mathbf{P}_i$ is the coordinate orthogonal to the tube contour axis and $K = 1\text{–}3Z/2(N\text{–}1)$. Details of the governing equation and the forces can be found in Xu *et al.* (2006).

B. Algorithm

A simulation is performed by evaluating the time evolution of an ensemble of N_C polymer chains and their associated confining tubes. The tube segments associated with a chain are paired with tube segments on different chains to simulate pairwise entanglements. At each time step, the forces and friction coefficients of each bead in Eq. (1) are evaluated from the chain conformation, after which the new position of each bead is obtained by integrating Eq. (1) forward in time using an Euler forward difference scheme. The time step is adjusted if necessary, based on the segmental extension, to ensure that finite extensibility is maintained; the Brownian force is adjusted consistently using Eq. (4) to ensure that the fluctuation-dissipation theorem is satisfied. The complete equation set used for the numerical integration is in Appendix B of Xu *et al.* (2006). The tube segments are then moved affinely by the flow field, as follows:

$$\mathbf{U}_z(t) = \exp\left[\int_{t'}^{t} \kappa(t'')dt''\right] \cdot \mathbf{U}_z(t'). \tag{8}$$

Here, $\lceil\rceil$ is a time-ordering operator, as defined by Van Kampen (1992).

The lengths of the end tube segments are adjusted to correspond to the positions of the first and last beads in the tube, which may not correspond to the first and Nth beads on the chain because of the possibility of chain loops. If the chain has retracted sufficiently to leave the end segment empty, the segment is removed and a constraint is released. If a chain reptates out of the existing tube, and the resulting end tube segment is less than or equal to the equilibrium tube segment length L_{eq}, the tube segment is extended to incorporate the chain. If the extended tube segment is greater than L_{eq}, the existing tube is cut at a length L_{eq} and a new tube segment with a randomly chosen orientation is created.

The re-entanglement algorithm then follows. An end tube segment that has been removed releases the conjugate constraint on another tube, and the two tube segments that meet at the conjugate constraint are combined. A newly created tube segment creates a conjugate constraint at the midpoint of a randomly chosen tube that is longer than L_{eq}. The details of these processes are modified in the new model, and they are described in the next section.

After rearrangement of the tube segments, the stress, $\boldsymbol{\tau}$, is obtained by ensemble averaging using the following Kramers formula:

$$\boldsymbol{\tau} = \sum_{i=1}^{N-1} \left\langle \mathbf{F}_i^S (\mathbf{R}_{i+1} - \mathbf{R}_i) \right\rangle - \sum_{i=1}^{N-1} \left\langle \mathbf{F}_i^T \mathbf{u}_i (s_{i+1} - s_i) \right\rangle - \sum_{i=1}^{N} \alpha_i \langle \mathbf{P}_i \mathbf{P}_i \rangle + n k_B T \boldsymbol{\delta}. \quad (9)$$

The new entanglements are rejected, and the process of tube creation is repeated in the event that finite extensibility is violated for any chain during this process.

C. Modification of the XDS simulator of Xu *et al.*

The problematic issues identified in the simulation results obtained from the previous XDS model of Xu *et al.* (2006) revolve around excessive predicted orientation and stretch. Any contemplated modification to the model must therefore simultaneously attenuate the stretch and reduce the orientation while simultaneously preserving all of the positive results from the model for $\dot{\gamma}\tau_e \leq 1$, where the entanglement microstructure is near equilibrium. We found that the re-entanglement process needs to be revised to prevent overstretching the newly created tubes and to preserve the total contour length of tubes in the ensemble. We also permitted the friction coefficient to be a function of the orientation of the bead/connectors relative to that of the surrounding matrix to reflect changes in the chain orientation; changing the friction coefficient simultaneously impacts the orientation, since the disengagement time decreases, and the stretch, since the longest Rouse time decreases. The two modifications are described below.

Figure 2 shows how the re-entanglement process is implemented**.** Here, L is the length of a tube segment, subscripts denote the index of each tube segment, and superscripts indicate whether the segment is *old* (before the re-entanglement process) or *new* (after the re-entanglement process). The differences in the contour lengths of the tubes after the constraint release and creation are ΔL^{CR} and ΔL^{CC}, respectively.

For the constraint release process, the *old* tube segment 2 is released by the removal of its conjugate segment at one of the ends of another tube. The *old* tube segment 2 is then combined with its neighboring *old* tube segment 1 to become a *new* tube segment 1. As a result, ΔL^{CR} is negative.

For the constraint creation process, a newly created tube segment at one of the ends of a tube is randomly conjugated with *old* tube 3, where it creates a new constraint and *new* tubes 3 and 4. Unlike the constraint release process, there are two degrees of freedom, the orientation and the length, in creating the new constraint. A random vector that is

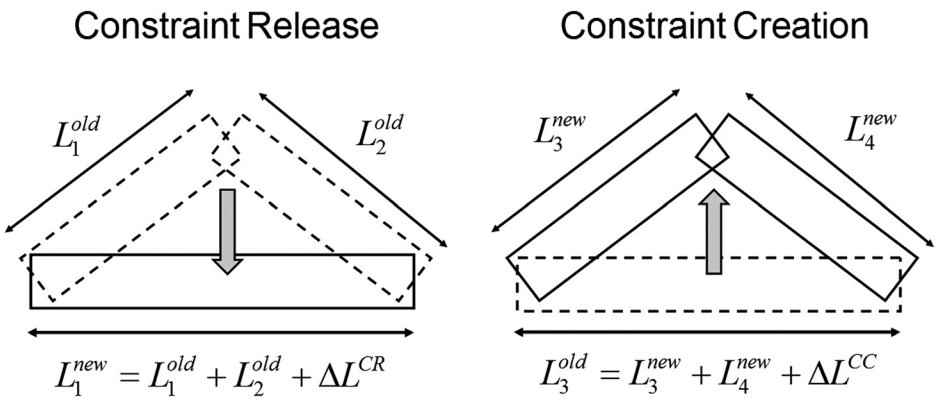

FIG. 2. Schematic diagram of the re-entanglement process (constraint release and creation) in the stochastic tube model: Dashed-line rectangles represent old tubes and solid-line rectangles are new tubes after the process.

perpendicular to the orientation of the *old* tube is selected. For the previous XDS model, ΔL^{CC} was chosen to be the average of the reduced contour lengths resulting from the constraint release process,

$$\Delta L^{CC} \equiv \langle \Delta L^{CR} \rangle = \sum_{l}^{N^{CR}} \Delta L_l^{CR} / N^{CR}. \tag{10}$$

Here, the index l represents each constraint release event, and N^{CR} denotes the total number of constraint release events. We found that the algorithm sometimes fails at very high shear rates and results in the divergence of the total contour length and overstretching of chains. To prevent divergence we modified the re-entanglement algorithm slightly, as follows:

$$\Delta L^{CC} \equiv \sum_{l}^{N^{CR}} \Delta L_l^{CR} / N^{CC}. \tag{11}$$

Here, N^{CC} is the number of newly created tube segments. This algorithm keeps the total contour length of the tubes in an ensemble constant during the re-entanglement process. The new entanglements are rejected and the process of tube creation is repeated in the event that finite extensibility is violated for any chain during this process.

We postulate that the beads and connectors can slide past one another more easily when they are highly aligned with the entanglement matrix. Conversely, when the bead connectors are crossed with the matrix entanglements, they cannot simply slide past the matrix entanglements; they must go around them because of the topological uncrossibility constraint. It would thus seem that the additional motion required to move around a nonaligned matrix, or, alternatively, cooperative motion between the segments, should manifest itself in a higher friction coefficient relative to the case where the bead connectors and the matrix entanglements are highly aligned and can simply slide past one another. Hence, we assume that the relative orientation of the connectors and the matrix polymer has a direct impact on the friction coefficient encountered by the beads. We are effectively accounting for changes in the friction coefficient as the entanglement microstructure changes, which is conceptually similar to an idea first advanced by Giesekus

many years ago [cf. Giesekus (1966, 1982, 1983); Larson (1988); Wiest (1989)]. (This proposed mechanism was alluded to in the Conclusion section of Xu *et al*. (2006). The relation between the Giesekus approach to anisotropic friction and a tensor drag coefficient employed by Curtiss and Bird (1981) to obtain reptationlike chain motion without employing the tube construct is discussed by Bird and Wiest (1985). More recently, Yaoita *et al*. (2008) varied the friction coefficient according to the number of Kuhn steps in each entanglement; these authors claimed that their algorithm is similar to that used in the CUBS model of Schieber *et al*. (2007). The latter concepts are different from our approach.) We emphasize that the qualitative mechanism for CDFC described here does not require nonaffine deformation of the tube segments (entanglements); the tube segments always deform affinely in our model. The chain segments captured within the tubes do deform nonaffinely, however, since the chains can retract into more interior tube segments upon deformation, and it is the variable effective friction involved in this dynamic retraction process that we address.

The average orientation of the matrix entanglements, $\mathbf{S}$, is given by

$$\mathbf{S} = \frac{1}{N_C N} \sum_j \sum_i \mathbf{q}_{j,i} \mathbf{q}_{j,i} - \frac{1}{3}\boldsymbol{\delta}. \tag{12}$$

Here, the unit vector $\mathbf{q}_i = \mathbf{Q}_i/|\mathbf{Q}_i|$, where $\mathbf{Q}_i = \mathbf{R}_i - \mathbf{R}_{i+1}$. The index j runs over the entire ensemble of chains, whereas the index i runs over the series of connectors on each chain. Since the number of Kuhn bonds in each connector is identical, there is no need for a weighting function. $\mathbf{S} = \mathbf{0}$ at equilibrium. We propose that the friction coefficient ζ_i, experienced by the ith bead is directly related to the relative orientations of the connector vectors between ith and $(i+1)$th beads and the matrix entanglements, $\mathbf{S}$, by the following relationship, which is chosen for its simplicity:

$$\zeta_i = \zeta_{eq}\left[1 - k\left(\frac{3}{2}\mathbf{q}_i\mathbf{q}_i : \mathbf{S}\right)\right]. \tag{13}$$

Here, ζ_{eq} is the friction coefficient in an isotropic, randomly oriented matrix. The factor 3/2 is a normalization constant such that $\frac{3}{2}\mathbf{q}_i\mathbf{q}_i : \mathbf{S}$ has the limiting value of unity for perfect alignment of the connectors with the matrix. The factor $0 \le k < 1$ is an empirical parameter that scales the magnitude of the topological effects. The friction coefficient is effectively constant at or very near equilibrium, with $\zeta_i = \zeta_{eq}$. Thus, the modified model collapses to the previous XDS model near equilibrium. Only when significant orientation of the matrix has occurred will the CDFC have an impact on model predictions. Both the Rouse time and the reptation time will be reduced by the proposed variation in the friction coefficient as a function of the entanglement microstructure, which will have the effect of simultaneously reducing the overalignment and stretch at high shear rates.

D. Model parameters

The previous XDS model had only one adjustable parameter, the characteristic time τ_H, which is proportional to the Rouse time:

$$\tau_H = \frac{\pi^2}{4N(N-1)}\tau_R. \tag{14}$$

The characteristic time scale is also proportional to the friction coefficient $\zeta_{eq} = 4H\tau_H$. τ_H is determined from a single experiment, which would typically be a linear viscoelastic experiment or a steady shear experiment at low rates. The number of tube segments at equilibrium, Z_{eq}, is determined using the relationship quantifying the number of entanglements in a monodisperse solution,

$$Z_{eq} = \phi^x \frac{M_w}{M_e}. \tag{15}$$

Here, ϕ is the volume fraction of the polymer, M_w is the molecular weight of the polymer, and M_e is the molecular weight between the entangled segments. The solvent quality exponent, x, was taken to be 1.2 for polystyrene solutions in Xu *et al.* (2006) and Hua and Schieber (1998), and that value is used in the simulations reported here. The molecular weight between entanglements is taken from Ferry (1980), and the Kuhn step length from Birshtein and Ptitsyn (1966) and Flory (1969).

Between 1000 and 3000 chains were used for each simulation. The computational parameters N and Δt were chosen as $4Z_{eq} + 1$ and $0.01 \sim 0.02\tau_H$, respectively, based on the convergent simulation results in Xu *et al.* (2006). For CDFC, the empirical parameter k in Eq. (13) was chosen to provide the best fit to the experimental data sets in transient and steady deformation. An equilibrium configuration was achieved by performing a simulation with zero deformation.

E. Experimental data sets

In this work, predicted results from the modified stochastic and analytical models were compared with the experimental data of nearly monodispersed entangled polymer solutions and melts. The material properties of the experimental data sets used in this study are listed in Table I.

To simulate the experimental data by the stochastic model, the model parameters were estimated as described in Sec. II D. The estimated simulation parameter sets are summarized in Table II. Note that for the stochastic simulation with modification by CDFC, $k = 0.99$ was found to give the best agreement with the experimental data. The selected functional form would therefore result in a 100-fold decrease in the frictional drag in the (unattainable) limit of full-chain extension and perfect alignment, where the tube construct would cease to be meaningful.

TABLE I. Material properties of the experimental data sets used to compare with predictions from the models studied in this paper.

Set name	M_w ($\times 10^6$ g/mol)	Poly-dispersity Index	Concentration (vol. %)	Solvent	Reference
Polystyrene PS-K	1.9	1.2	13	Tricresyl phosphate	Kahvand (1995) and Venerus and Kahvand (1994)
Polystyrene PS-O	8.42	1.17	5	Tricresyl phosphate	Oberhauser *et al.* (2004).
Polystyrene PS-B	10.2	1.17	6	Dibutyl phthalate	Bhattacharjee *et al.* (2003)
Polystyrene PSM	0.2	1.05	100	Melt	Bach *et al.* (2003)
Polystyrene PS-Y	8.42	1.17	7	Tricresyl phosphate	Ye *et al.* (2003)

TABLE II. Parameter sets for the stochastic model to simulate the experimental data sets. Estimates were made as described in Sec. II D.

Set name	Z_{eq}	τ_R (s)	Flow type
PS-K	9	1.27	Shear
PS-O	13	4.52	Shear
PS-B	21	2.3	Uniaxial extension
PSM	11	57	Uniaxial extension

III. COMPARISON OF RESULTS FROM THE MODIFIED MODEL TO EXPERIMENTAL DATA

A. Shear flows of entangled polymers

Xu *et al.* (2006) simulated the shear data of Venerus and Kahvand (1994) and Kahvand (1995) for an entangled polystyrene solution denoted as PS-K in Tables I and II. As shown in Figs. 3 and 4, the simulation results from their stochastic tube model are in a good agreement with the experimental data for the shear viscosity η and the first normal stress difference coefficient Ψ_1 from low to moderate shear rates. There is a systematic deviation from the experimental data as the shear rate is increased, however, and both η and Ψ_1 are significantly overestimated for shear rates greater than about $8\,s^{-1}$ ($\dot{\gamma}\tau_R > 10$). Figures 3 and 4 also show simulations using the modifications described in Sec. II. The use of Eq. (11) in the re-entanglement algorithm without CDFC ($k=0$) results in some improvement in η at $\dot{\gamma}\tau_R > 0.5$ and removes much of the overestimation for $\dot{\gamma}\tau_R > 10$. The results including CDFC, where $k=0.99$ gives the best result, show very good agreement with the data.

Figures 5 and 6 show the simulations of the transient shear viscosity η^+ and the transient normal stress difference coefficient $\Psi_1{}^+$, respectively. The methods are all

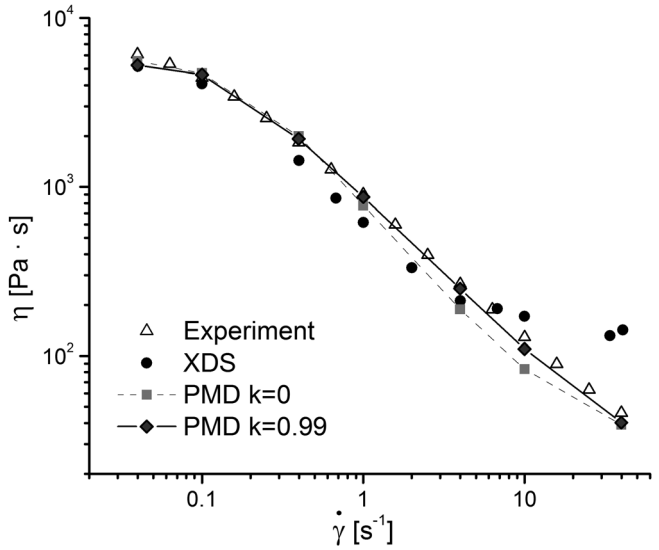

FIG. 3. Steady shear viscosity as a function of shear rate: Comparison between the experimental data of polystyrene solution PS-K [Venerus and Kahvand (1994); Kahvand (1995)] and the simulation results from the previous XDS model [Xu *et al.* (2006)] and the modified PMD models with/without CDFC ($k=0.99/0$). Lines are drawn to guide the eye.

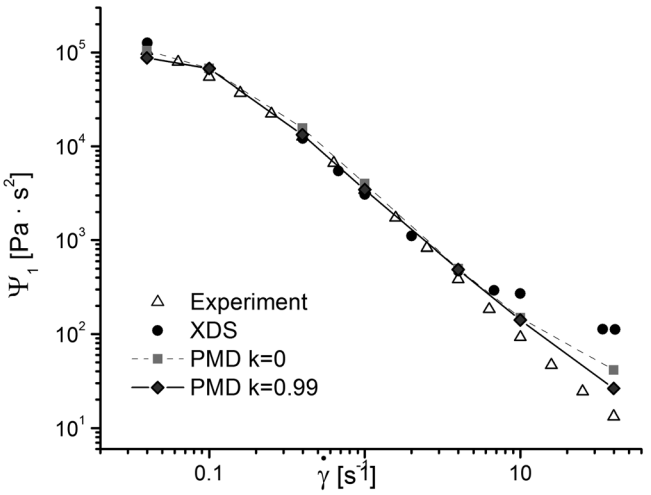

FIG. 4. Steady normal stress difference coefficient as a function of shear rate: Comparison between the experimental data of polystyrene solution PS-K [Venerus and Kahvand (1994); Kahvand (1995)] and simulation results from the previous XDS model [Xu *et al.* (2006)] and the modified PMD models with/without CDFC ($k = 0.99/0$).

equivalents at a shear rate of $0.1\,s^{-1}$, and all predict the transient data well. At $1\,s^{-1}$, however, the simulation results from the XDS model of Xu *et al.* (2006) begin to deviate from the transient viscosity data, while the modified model both with and without CDFC remain in agreement. The differences in the results from each simulation method became apparent at a shear rate of $40\,s^{-1}$ ($\dot{\gamma}\tau_R \gg 10$). The predictions of the XDS model are indicated by the arrows in Figs. 5 and 6; the deviation from the data is significant, and the predictions are in fact quite similar to those for $4\,s^{-1}$. The computed steady-state viscosity from the modified model without CDFC is in a good agreement with the data, but the calculated maximum in the transient is much larger than the experimental value. The

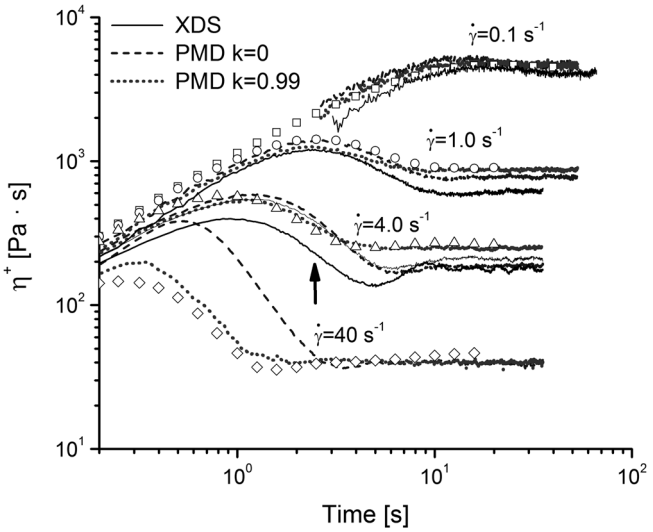

FIG. 5. Transient shear viscosity as a function of time at various shear rates: Comparison between the experimental data of polystyrene solution PS-K [Venerus and Kahvand (1994); Kahvand (1995)] and the simulation results from the previous XDS model [Xu *et al.* (2006)] and the modified PMD models with/without CDFC ($k = 0.99/0$). The arrow indicates simulation results from the XDS model at a shear rate of $40\,s^{-1}$.

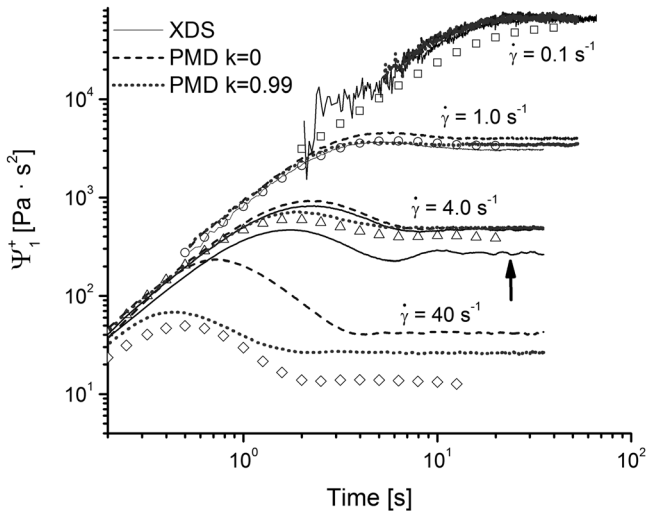

FIG. 6. Transient normal stress difference coefficient as a function of time at various shear rates: Comparison between the experimental data of polystyrene solution PS-K [Venerus and Kahvand (1994); Kahvand (1995)] and the simulation results from the previous XDS model [Xu *et al.* (2006)] and the modified PMD models with/without CDFC ($k = 0.99/0$). The arrow indicates simulation results from the XDS model at a shear rate of $40\,s^{-1}$.

simulation result with CDFC using $k = 0.99$, by contrast, shows a good agreement with the data over the entire transient. The agreement between the simulation and the transient normal stress coefficient is not as good at $40\,s^{-1}$, but it is a considerable improvement over the XDS prediction or the modified calculation without CDFC.

Xu *et al.* (2006) also simulated the shear flow of an entangled polystyrene solution studied by Oberhauser *et al.* (2004), denoted as PS-O in Tables I and II. Figure 7 shows very good agreement between the CDFC simulation of the viscosity with $k = 0.99$ and

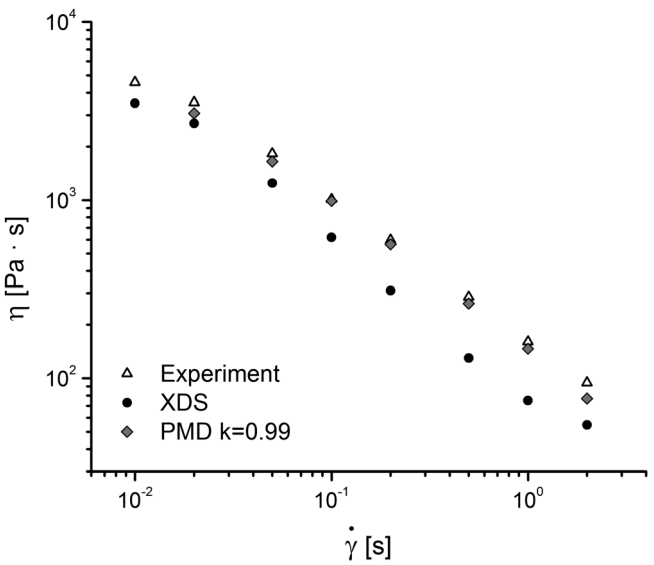

FIG. 7. Steady shear viscosity as a function of shear rate: Comparison between the experimental data of a polystyrene solution PS-O [Oberhauser *et al.* (2004)] and the simulation results from the previous XDS model [Xu *et al.* (2006)] and the modified PMD model with CDFC ($k = 0.99$).

the experimental data, whereas there is a systematic deviation over most of the experimental range, which corresponds to $\dot{\gamma}\tau_R \leq 10$, with the XDS model. The predictions of the first normal stress coefficient with both formulations shown in Fig. 8 are similar and are in good agreement with the data.

B. Extensional flows of entangled polymers

We now turn to the simulation of steady and transient uniaxial extension, and we employ only the modified model [i.e., with Eq. (11)] with and without CDFC. Figure 9 shows extensional stress data as a function of strain at two stretch rates for an entangled polystyrene solution denoted as PS-B, which was studied by Bhattacharjee *et al*. (2003); the steady-state Trouton ratio (extensional viscosity/zero-shear viscosity) is shown in Fig. 10. The model overestimates most of the transient data, but it predicts the steady state very well with CDFC and $k = 0.99$, including capturing the initial power-law exponent of -0.5 followed by strain hardening. The use of CDFC is required to predict the -0.5 scaling and the presence of a minimum; the data are overestimated over the entire range with $k = 0$. Clearly, CDFC provides an accelerated relaxation mechanism at high stretch rates ($\dot{\varepsilon}\tau_R > 1$) to relieve the overstretching of the chains.

Figures 11 and 12 show transient and steady-state extensional data by Bach *et al*. (2003) for a polystyrene melt (PSM). The simulation with $k = 0.99$ shows the -0.5 scaling and is in agreement with the experiments at low extension rates, but it predicts a minimum and subsequent strain hardening at high extension rates, whereas the data show a -0.5 scaling over a broad range of extension rates up to and including $\dot{\varepsilon}\tau_R \approx 1$. The stochastic simulator with CDFC falls within the class of molecular models that Marrucci and Iannirubertо (2004) refer to as "standard" tube constructs, and it appears that such models cannot capture the broad -0.5 power-law scaling observed by Bach *et al*. (2003). We believe that the -0.5 regime represents a transition from the zero-shear viscosity slope of zero to an asymptotic -1 power law that is not observed in standard models,

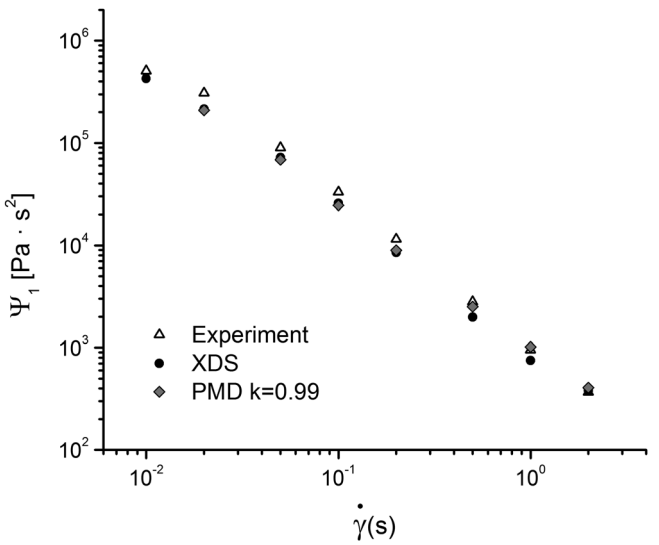

FIG. 8. Steady shear normal stress difference coefficient as a function of shear rate: Comparison between the experimental data of polystyrene solution PS-O [Oberhauser *et al*. (2004)] and the simulation results from the previous XDS model [Xu *et al*. (2006)] and the modified PMD model with CDFC ($k = 0.99$).

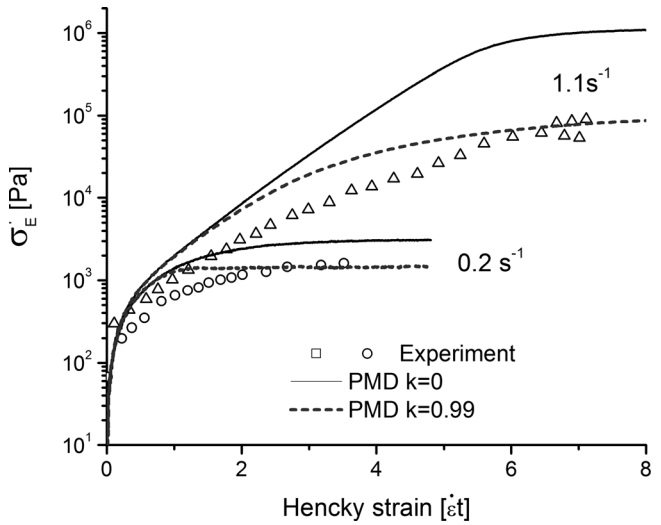

FIG. 9. Transient extensional stress at various strain rates: Comparison between the experimental data of polystyrene solution PS-B [Bhattacharjee *et al*. (2003)] and the simulation results from the modified PMD models with/without CDFC ($k = 0.99/0$).

because it is cut off by the inception of strain hardening. Wagner *et al*. (2005) have constructed a "nonstandard" model based on the "interchain pressure" concept of Marrucci and Ianniruberto (2004), which causes a resistance to squeezing the tube diameter during extensional flow, and the idea has been further developed by Wagner *et al*. (2008) and Dhole *et al*. (2009); this approach does capture the -0.5 scaling over a broad range of extension rates. A recent study by Kushwaha and Shaqfeh (2011) presents an alternative explanation for the scaling based on disentanglement during extension.

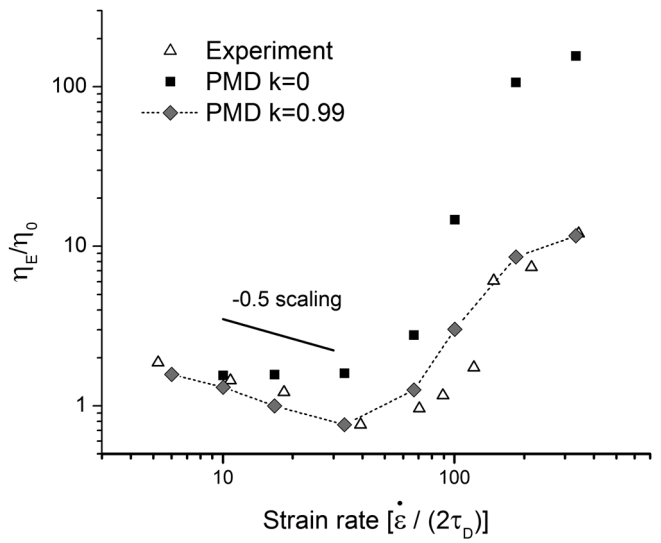

FIG. 10. Steady-state extensional viscosity as a function of strain rate (normalized by $2\tau_D$): Comparison between the experimental data of polymer solution PS-B [Bhattacharjee *et al*. (2003)] and the simulation results from the modified PMD models with/without CDFC ($k = 0.99/0$). Lines are drawn to guide the eye.

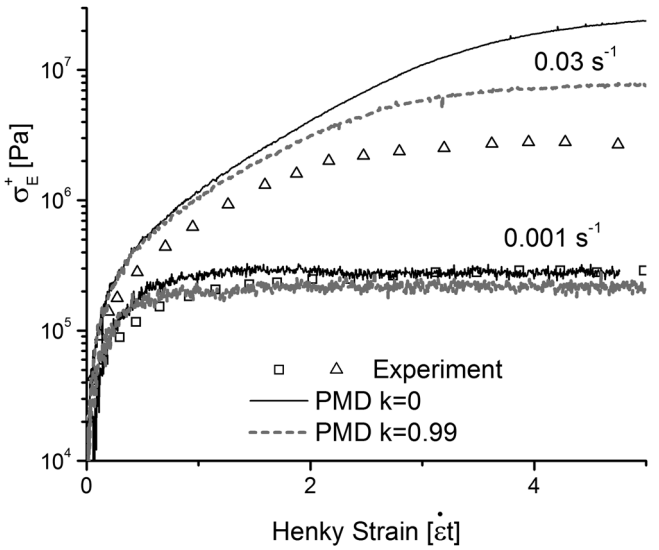

FIG. 11. Transient extensional stress at various strain rates: Comparison between the experimental data of PSM [Bach *et al*. (2003)] and the simulation results from the modified PMD models with/without CDFC ($k = 0.99/0$).

IV. COMPARISON WITH THE MLD MODEL

The success of CDFC in improving the predictions of the stochastic model raises the question as to whether this is in fact a universal phenomenon for entangled polymers. We therefore applied CDFC to the MLD toy model, which is a simplified version of the full MLD model at the tube coordinate level [Mead *et al*. (1998); Mead (2007)]. The CDFC was incorporated into the MLD model by changing the characteristic relaxation time

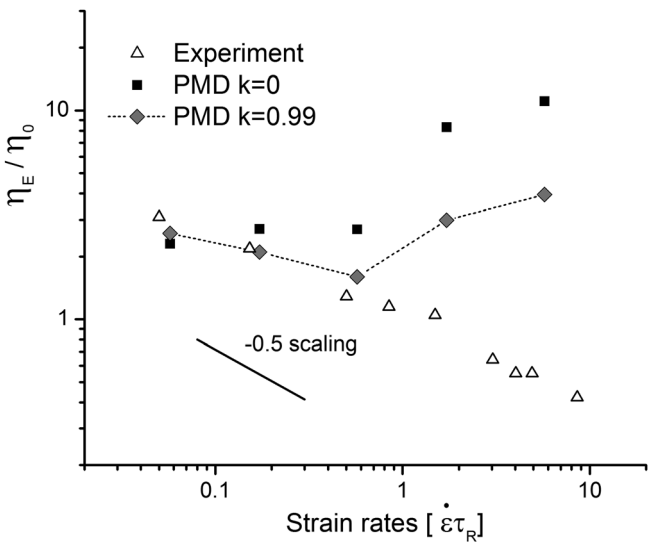

FIG. 12. Steady extensional viscosity at various strain rates: Comparison between the experimental data of PSM [Bach *et al*. (2003)] and the simulation results from the modified PMD models with/without CDFC ($k = 0.99/0$).

scale input parameters (τ_R and τ_D) using the order parameter tensor $\mathbf{S}'$ (defined as $\mathbf{S}$ in the original paper), defined as follows:

$$\tau = \tau_{eq}\left[1 - k\left(\frac{3}{2}\mathbf{S}' : \mathbf{S}'\right)\right]. \tag{16}$$

Here, the subscript *eq* indicates the input value at equilibrium.

Table III summarizes the experimental data sets used for comparison with the predictions of the MLD model when CDFC is incorporated, as well as the input parameters used for the calculations. The number of entanglements Z_{eq} and the extensibility parameter, β, which is the ratio between L_{eq} and the maximum stretch of a tube segment, were estimated as described by Pattamaprom and Larson (2001) and Fetters *et al.* (1994). The plateau moduli G_N^{O} and τ_R for PS-B and PS-Y were taken from the original references. τ_R of PS-K was estimated by fitting the linear viscoelasticity data, as described in Sec. II D and Xu *et al.* (2006), and G_N^{O} was selected to provide the best fit to the experimental data.

Figures 13 and 14 show the MLD simulations with CDFC of the transient viscosity and first normal stress coefficient, respectively, for PS-K at $40\,\mathrm{s}^{-1}$. We have chosen this shear rate for illustration, because it represents the most difficult case. The final steady-state viscosity is predicted reasonably with all values of k, but both the position and magnitude of the maximum are greatly overestimated with $k = 0$. The viscosity data are fit very well with $k = 0.8$ but underestimated by $k = 0.99$. The fit to the normal stress coefficient with $k = 0$ is very poor, with the fit improving as k is increased to a value of 0.8. The steady-state values of both η and Ψ_1 are fit very well over the entire shear rate range with $k = 0.8$.

Ye *et al.* (2003) simulated their polystyrene PS-Y extensional data using the MLD model. They adjusted the extensibility parameter, β, which is a ratio between L_{eq} and the maximum stretch of a tube segment, to obtain agreement with the experimental data at a high strain rate, as shown in Fig. 15; the original estimate of β was 0.056, but they employed a value of 0.12. The extensional viscosity was significantly overestimated over most of the experimental range in any event, although less so with $\beta = 0.12$ than with $\beta = 0.056$. Figure 15 shows the result from the MLD model including CDFC using the same parameter values as Ye *et al.*, but with $\beta = 0.056$ and $k = 0.4$. The agreement with the data is improved considerably without the need to adjust β in a nonphysical way.

Simulations of the extensional flow data of Bhattacharjee *et al.* (2003) on polystyrene PS-B using the MLD model with and without CDFC are shown in Figs. 16 and 17. The estimate of β for this solution is 0.043, but it must be increased (in this case to 0.096) in order to approach the data at high rates without incorporating CDFC. The fit to the data with $\beta = 0.043$ is quite good when CDFC is incorporated, however, with $k = 0.4$. Larger values of k significantly underestimate the extensional viscosity at high rates.

We also applied the MLD model with and without CDFC to the extensional flow melt data of Bach *et al.* (2003) on PSM. The predictions were similar to those of the stochastic

TABLE III. Experimental data sets and corresponding parameter sets for the MLD predictions.

Set name	G_N^O (Pa)	Z_{eq}	τ_R (s)	τ_D (s)	β	Estimation method
PS-K	1000	9	1.27	7.5	0.060	Xu *et al.* (2006) and Pattamaprom and Larson (2001)
PS-B	290	25	2.96	83.66	0.043	Bhattacharjee *et al.* (2003)
PS-Y	480.4	36	5.0	189.6	0.056	"Toy model data set" in Ye *et al.* (2003)

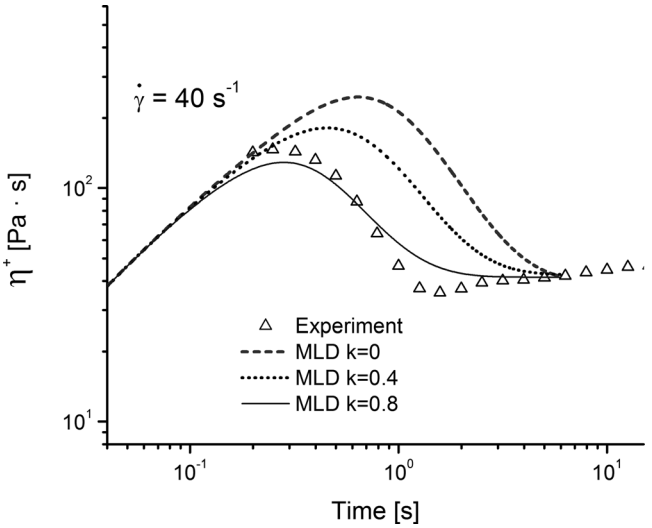

FIG. 13. Transient shear viscosity as a function of time at a shear rate of $40\,s^{-1}$: Comparison between the experimental data of polystyrene solution PS-K [Venerus and Kahvand (1994); Kahvand (1995)] and the predictions of the original toy MLD model [Mead *et al*. (1998)] and its modifications by CDFC ($k = 0.4$ and 0.8).

model, and we were unable to predict the absence of extension thickening; increasing k delayed the upturn, but at the expense of increasing the deviation from the data at low rates.

Overall, the MLD model with CDFC gave results that were consistent with and comparable to the stochastic model with CDFC and considerably better than the original MLD model. The stochastic model results were obtained with $k = 0.99$, however, while smaller values, ranging from 0.4 to 0.8, were required for the MLD model. This

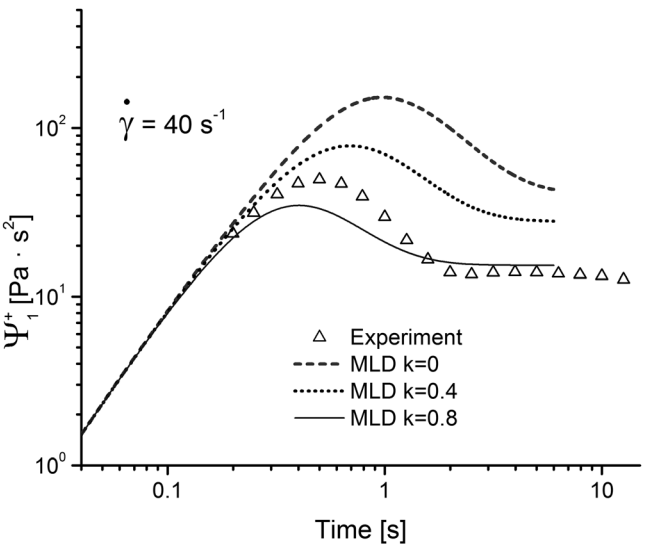

FIG. 14. Transient normal stress difference coefficients as a function of time at a shear rate of $40\,s^{-1}$: Comparison among the experimental data of polystyrene solution PS-K [Venerus and Kahvand (1994); Kahvand (1995)], and the predictions of the original toy MLD model [Mead *et al*. (1998)] and its modifications by CDFC ($k = 0.4$ and 0.8).

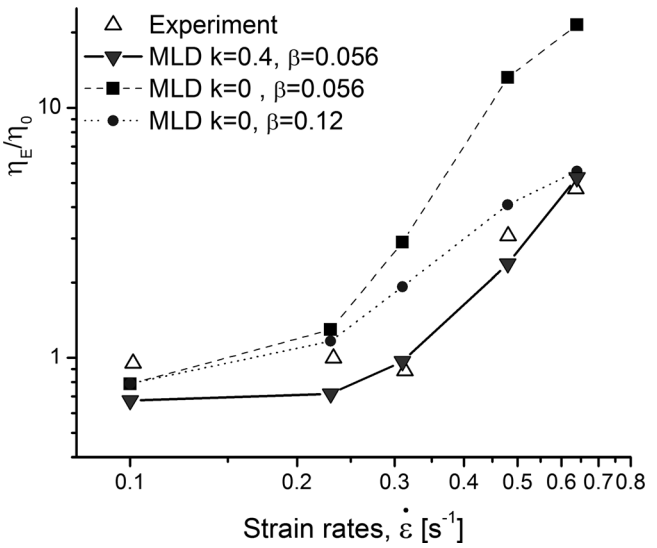

FIG. 15. Steady-state extensional viscosity as a function of strain rate: Comparison between the experimental data of polymer solution PS-Y [Ye *et al*. (2003)] and predictions of the original MLD model ($k = 0$, $\beta = 0.056$), the MLD model with adjustment of extensibility ($k = 0$, $\beta = 0.12$), and the MLD model with CDFC ($k = 0.4$, $\beta = 0.056$). Lines are drawn to guide the eye.

difference is not surprising. The stochastic simulator calculates the reduction in frictional drag based on the relative orientation of individual chains, whereas the MLD model calculates the reduction using the order parameter tensor, which is an averaged quantity. The order parameter tensor overestimates the relative orientation of individual chains. Hence, we would expect that k must be lower in the MLD model relative to the stochastic simulator.

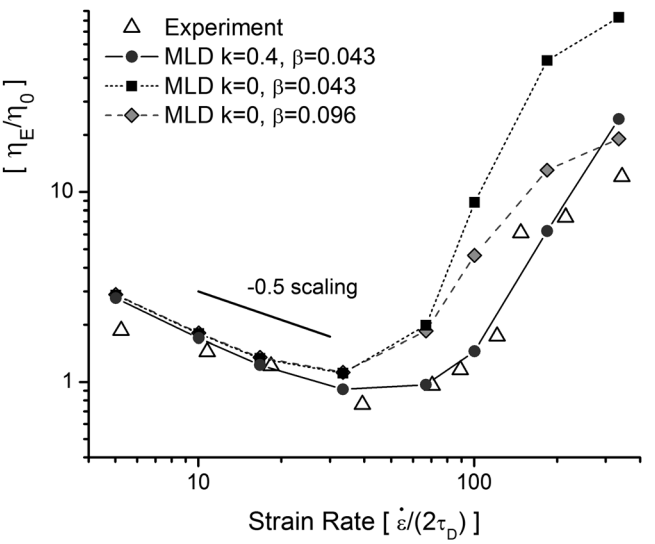

FIG. 16. Steady-state extensional viscosity as a function of strain rate (normalized by $2\tau_D$): Comparison between the experimental data of polymer solution PS-B [Bhattacharjee *et al*. (2003)] and predictions of the original MLD model ($k = 0$, $\beta = 0.043$), the MLD model with adjustment of extensibility ($k = 0$, $\beta = 0.096$), and the MLD model with CDFC ($k = 0.4$, $\beta = 0.043$). Lines are drawn to guide the eye.

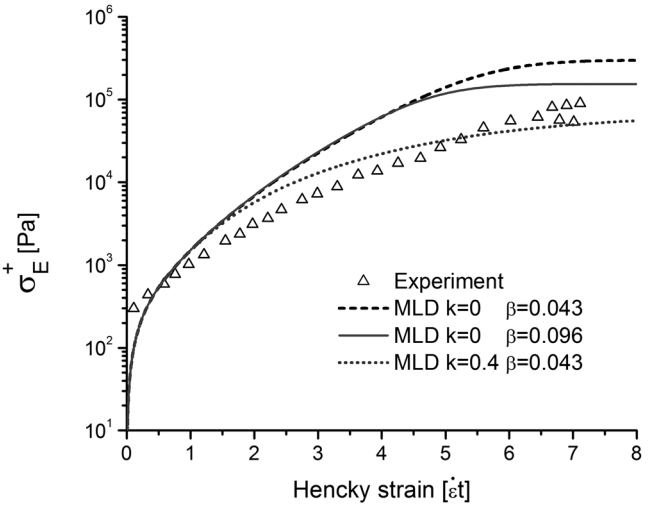

FIG. 17. Transient extensional stress at a rate of $1.1\,s^{-1}$ as a function of Hencky strain: Comparison between the experimental data of polymer solution PS-B [Bhattacharjee *et al.* (2003)] and predictions of the original MLD model ($k=0$, $\beta=0.043$), the MLD model with adjustment of extensibility ($k=0$, $\beta=0.096$), and the MLD model with CDFC ($k=0.4$, $\beta=0.043$).

V. CONCLUSIONS

We are able to improve the simulation of high shear rate data by slightly modifying the re-entanglement algorithm in the XDS stochastic model of Xu *et al.* (2006) in order to ensure conservation of the total length of tubes during constraint release and creation. The major improvement of our PMD stochastic model, however, comes from including a configuration-dependent friction coefficient into the algorithm to account for changes in the entanglement microstructure far from equilibrium. In that case, the stochastic model is able to do an effective job of simulating both shear and extensional stress data over a wide range of deformation rates. Incorporation of CDFC accelerates the relaxation process at high rates. The parameter k is in principle adjustable, but a value close to unity, wherein the friction coefficient varies between the equilibrium value in weak flows and a very small value for perfect alignment, appears to be adequate for the polystyrene systems studied.

CDFC is not a new concept. It was incorporated into continuum modeling more than 30 years ago by Giesekus, and it is equivalent in its effect on relaxation to segment-scale nonaffine tube deformations that are contained in other models. The success in simulating nonlinear shear and extension data by incorporating CDFC into the stochastic model, which is a tool for exploring mechanisms at a segmental level, suggested that CDFC might be effective in continuum tube models, and that is indeed the case for the MLD model [Mead *et al.* (1998)]. CDFC is applied to an averaged quantity for the continuum model, and the best value of the parameter is smaller than unity. In this case, however, the number of adjustable parameters in the model remains unchanged, since the parameter that has been arbitrarily adjusted in the original MLD formulations no longer needs to be changed.

There have long been hints that relaxation processes may be speeded up in nonlinear flows, consistent with our simulation results. Attempts at measuring the dynamic moduli during nonlinear steady shear flow indicate that the relaxation modulus is cut off at the long time scales and decreases as steady shear is applied, although this result may partially be an orientational effect due to a decrease in orientation angle and not exclusively

due to entanglement microstructure modification (reduction) [Booij (1966, 1968); Simmons (1968); Somma *et al*. (2007)]. Further experimental work in this area to guide and direct theoretical studies would be helpful.

The two tube models studied here differ in one significant way: The entanglement density in the stochastic simulator decreases with the rate of deformation, whereas it is constant in the MLD model, yet both formulations, when incorporating CDFC, give nearly equivalent predictions for shear and extensional data. Furthermore, the entanglement density can increase in the GLaMM molecular model [Graham *et al*. (2003)]. The stochastic model enables us to "turn on or off" various physical mechanisms easily, and we have briefly explored this issue of the microstructural changes in tube segments in fast flows in terms of the entanglement dynamics. These results are summarized in the Appendix.

ACKNOWLEDGMENTS

This work was supported by NSF Grant No. 0625072. The authors are grateful to Dr. Fang Xu and Professor J. D. Schieber for helpful discussions and comments.

APPENDIX: ENTANGLEMENT DENSITY DYNAMICS

All models of entangled polymers predicted a constant entanglement density ($\langle Z \rangle \approx Z_{eq}$) in the linear viscoelastic limit that is effectively defined by the plateau modulus [Fetters *et al*. (1999)]. The plateau modulus defines the fundamental length scale (molecular weight between entanglements) and is arguably the most basic parameter in any molecular model of entangled polymers [Tzoumanekas and Theodorou (2006)]. What happens to the modulus, and consequently the fundamental entanglement length scale, far from equilibrium is not yet fully understood. More specifically, whether the entanglement density changes in fast dynamic flow situations is still an open question. We can define three distinct categories of molecular models on the basis of the predicted entanglement density in fast flows:

(1) Decreased entanglement density in fast nonlinear flows ($\langle Z \rangle < Z_{eq}$). This behavior is characteristic of most of the stochastic models, including the PMD stochastic model in this work and the antecedent XDS model of Xu *et al*. (2006) and the slip-link models of Doi and Takimoto (2003), Schieber *et al*. (2007), and Dambal *et al*. (2009).
(2) Constant entanglement density in fast nonlinear flows ($\langle Z \rangle = Z_{eq}$). The basic Doi–-Edwards model and its derivatives [Doi and Edwards (1986); Mead (1995a, 1995b); Pearson *et al*. (1991)] have a constant entanglement density independent of deformation rate or type, including the MLD model and all its derivatives [Mead *et al*. (1998); Mead (2007)].
(3) Increased entanglement density in fast nonlinear flows ($\langle Z \rangle > Z_{eq}$). The GLaMM model (which is subsequently recast into a closed deterministic form) predicts that the entanglement density increases as the chain stretches in fast flows [Graham *et al*. (2003)].

The stochastic model developed in this work affords an opportunity to test the importance of the entanglement density on the predicted rheological properties by adjusting the way in which the entanglement density is controlled. Following the re-entanglement process described in Sec. II C, $\langle Z \rangle$ is evaluated. If the goal is a constant entanglement density, $\big(Z_{eq} - \langle Z \rangle\big)N_C$ entangled segments must be newly created. For an increased entanglement density, Z_{eq} is multiplied by the average chain stretch relative to the

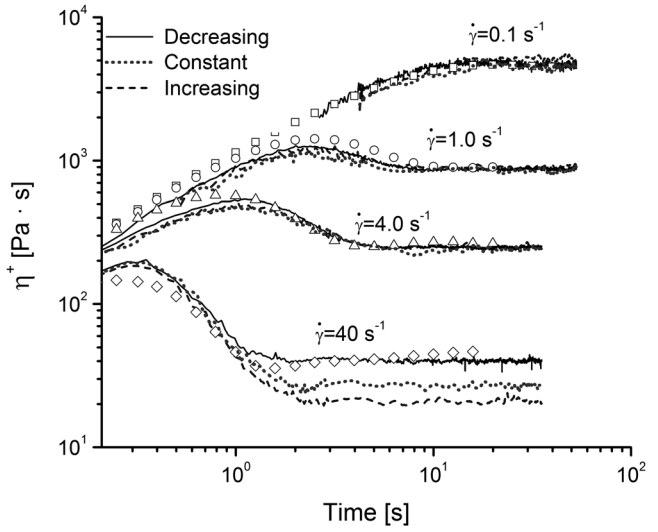

FIG. 18. Transient shear viscosity as a function of time at various shear rates: Comparison between the experimental data (symbols) of polystyrene solution PS-K [Venerus and Kahvand (1994); Kahvand (1995)] and the simulation results from the modified PMD models (CDFC $k = 0.99$) with entanglement density control algorithm (constant/increasing) and without (decreasing).

equilibrium chain length to determine the new value of $\langle Z \rangle$. These new entanglements are placed at randomly selected core segments, in contrast to the re-entanglement algorithm in the basic stochastic model, which always takes place between a tip and a core.

Simulation results for the transient viscosity and first normal stress coefficient data for the polystyrene solution PS-K of Kahvand (1995) are shown in Figs. 18 and 19, respectively, with a decreasing entanglement density (i.e., without any entanglement control), a constant entanglement density, and an increasing entanglement density. There is no

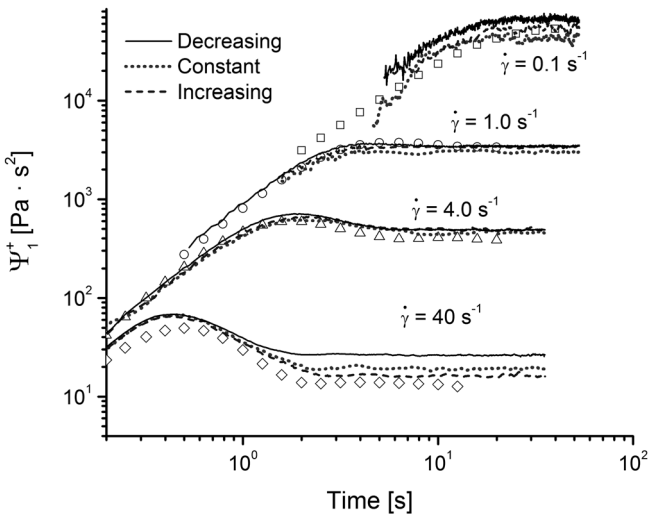

FIG. 19. Transient first normal stress coefficient as a function of time at various shear rates: Comparison between the experimental data (symbols) of polystyrene solution PS-K [Venerus and Kahvand (1994); Kahvand (1995)] and the simulation results from the modified PMD models (CDFC $k = 0.99$) with entanglement density control algorithm (constant/increasing) and without (decreasing).

significant difference between the three entanglement assumptions at shear rates up to $4\,s^{-1}$. At the very high shear rate of $40\,s^{-1}$, the transient shear data are best represented by a decreasing entanglement density and the transient normal stress data by an increasing entanglement density, but these are the most difficult data for the models considered in this work. It is not clear why the theoretically predicted rheological properties are so insensitive to such a seemingly fundamental parameter as the entanglement density, which characterizes the entanglement microstructure. This issue needs to be thoroughly addressed in future work. We do note in passing that the conventional view is that apparent wall slip in shear and rupture in rapid stretching are consequences of a reduction in entanglements. The recent study by Kushwaha and Shaqfeh (2011) proposed that the decreasing entanglement density may be related to the scaling of the extensional viscosity reduction at low to moderate strain rates. On the other hand, Malkin *et al*. (2011) have recently offered a provocative picture of entanglements that would suggest an increasing entanglement density.

References

Auhl, D., P. Chambon, T. C. B. McLeish, and D. J. Read, "Elongational flow of blends of long and short polymers: Effective stretch relaxation time," Phys. Rev. Lett. **103**, 136001 (2009).

Bach, A., K. Almdal, H. K. Rasmussen, and O. Hassager, "Elongational viscosity of narrow molar mass distribution polystyrene," Macromolecules **36**, 5174–5179 (2003).

Ball, R. C., and T. C. B. McLeish, "Dynamic dilution and the viscosity of star polymer melts," Macromolecules **22**, 1911–1913 (1989).

Bhattacharjee, P., D. Nguyen, G. McKinley, and T. Sridhar, "Extensional stress growth and stress relaxation in entangled polymer solutions," J. Rheol. **47**, 269–290 (2003).

Bird, R. B., and J. M. Wiest, "Anisotropic effects in dumbbell kinetic theory," J. Rheol. **29**, 519–532 (1985).

Birshtein, T. M., and O. B. Ptitsyn, *Conformations of Macromolecules* (Interscience, New York, 1966).

Booij, H. C., "Influence of superimposed steady shear flow on the dynamic properties of non-Newtonian fluids: I Measurements on non-Newtonian solutions," Rheol. Acta **5**, 215–221 (1966).

Booij, H. C., "Influence of superimposed steady shear flow on the dynamic properties of non-Newtonian fluids: III Measurements on oscillatory normal stress components," Rheol. Acta **7**, 202–209 (1968).

Burghelea, T. I., Z. Stary, and H. Munstedt, "Local versus integral measurements of the extensional viscosity of polymer melts," J. Rheol. **53**, 1363–1377 (2009).

Curtiss, C. F., and R. B. Bird, "A kinetic theory for polymer melts. I. The equation for the singlelink orientational distribution function," J. Chem. Phys. **74**, 2016–2025 (1981).

Dambal, A., A. Kushwaha, and E. S. G. Shaqfeh, "Slip-link simulations of entangled, finitely extensible, wormlike chains in shear flow," Macromolecules **42**, 7168–7183 (2009).

Denn, M. M., *Polymer Melt Processing: Foundations in Fluid Mechanics and Heat Transfer* (Cambridge University Press, New York, 2008).

Dhole, S., A. Leygue, C. Bailly, and R. Keunings, "A single segment differential tube model with interchain tube pressure effect," J. Non-Newtonian Fluid Mech. **161**, 10–18 (2009).

Doi, M., "Explanation for the 3.4-power law for viscosity of polymeric liquids on the basis of the tube model," J. Polym. Sci., Polym. Phys. Ed. **21**, 667–684 (1983).

Doi, M., and J.-I. Takimoto, "Molecular modeling of entanglements," Philos. Trans. R. Soc. London, Ser. A **361**, 641–650 (2003).

Doi, M., and S. F. Edwards, "Dynamics of concentrated polymer systems. Part 1. Brownian motion in the equilibrium state," J. Chem. Soc., Faraday Trans. 2 **74**, 1789–1801 (1978a).

Doi, M., and S. F. Edwards, "Dynamics of concentrated polymer systems. Part 2. Molecular motion under flow," J. Chem. Soc., Faraday Trans. 2 **74**, 1802–1817 (1978b).

Doi, M., and S. F. Edwards, "Dynamics of concentrated polymer systems. Part 3. The constitutive equation," J. Chem. Soc., Faraday Trans. 2 **74**, 1818–1832 (1978c).

Doi, M., and S. F. Edwards, "Dynamics of concentrated polymer systems. Part 4. Rheological properties," J. Chem. Soc., Faraday Trans. 2 **75**, 38–54 (1979).

Doi, M., and S. F. Edwards, *The Theory of Polymer Dynamics* (Oxford University Press, New York, 1986).

de Gennes, P. G., "Reptation of a polymer chain in the presence of fixed obstacles," J. Chem. Phys. **55**, 572–579 (1971).

Edwards, S. F., "Statistical mechanics with topological constraints: I," Proc. Phys. Soc. **91**, 513–519 (1967).

Edwards, S. F., and Th. Vilgis, "The effect of entanglements in rubber elasticity," Polymer **27**, 483–492 (1986).

Everaers, R., S. K. Sukumaran, G. S. Grest, C. Svaneborg, A. Sivasubramanian, and K. Kremer, "Rheology and microscopic topology of entangled polymeric liquids," Science **303**, 823–827 (2004).

Fang, J., M. Kröger, and H. C. Öttinger, "A thermodynamically admissible reptation model for fast flows of entangled polymers. II. Model predictions for shear and extensional flows," J. Rheol. **44**, 1293–1317 (2000).

Ferry, J. L., *Viscoelastic Properties of Polymers*, 3rd ed. (Wiley, New York, 1980).

Fetters, L. I., D. J. Lohse, D. Richter, T. A. Witten, and A. Zirhel, "Connection between polymer molecular weight, density, chain dimensions, and melt viscoelastic properties," Macromolecules **27**, 4639–4647 (1994).

Fetters, L. J., D. J. Lohse, and W. W. Graessley, "Chain dimensions and entanglement spacings in dense macromolecular systems," J. Polym. Sci., Part B: Polym. Phys. **37**, 1023–1033 (1999).

Flory, P. J., *Statistical Mechanics of Chain Molecules* (Interscience, New York, 1969).

Giesekus, H., "Die elastizitat von flussigkeiten," Rheol. Acta **5**, 29–35 (1966).

Giesekus, H., "A simple constitutive equation for polymer fluids based on the concept of deformation-dependent tensorial mobility," J. Non-Newtonian Fluid Mech. **11**, 69–109 (1982).

Giesekus, H., "Stressing behaviour in simple shear flow as predicted by a new constitutive model for polymer fluids," J. Non-Newtonian Fluid Mech. **12**, 367–374 (1983).

Gigras, P. G., and B. Khomami, "Adaptive configuration fields: A new multiscale simulation technique for reptation-based models with a stochastic strain measure and local variations of life span distribution," J. Non-Newtonian Fluid Mech. **108**, 99–122 (2002).

Graham, R. S., A. E. Likhtman, T. C. B. McLeish, and S. T. Milner, "Microscopic theory of linear entangled polymer chains under rapid deformation including chain stretch and convective constraint release," J. Rheol. **47**, 1171–1200 (2003).

Greco, F., "The stress tensor in entangled polymers," Phys. Rev. Lett. **88**, 108301 (2002).

Hua, C. C., and J. D. Schieber, "Segment connectivity, chain-length breathing, segmental stretch, and constraint release in reptation models. I. Theory and single step strain predictions," J. Chem. Phys. **109**, 10018–10027 (1998).

Hua, C. C., J. D. Schieber, and D. C. Venerus, "Segment connectivity, chain-length breathing, segmental stretch, and constraint release in reptation models. II. Double step strain predictions," J. Chem. Phys. **109**, 10028–10032 (1998).

Hua, C. C., J. D. Schieber, and D. C. Venerus, "Segment connectivity, chain-length breathing, segmental stretch, and constraint release in reptation models. III. Shear Flows," J. Rheol. **43**, 701–718 (1999).

Ianniruberto, G., and G. Marrucci, "On compatibility of the Cox–Merz rule with the model of Doi and Edwards," J. Non-Newtonian Fluid Mech. **65**, 241–246 (1996).

Joshi, Y. M., and M. M. Denn, "Rupture of entangled polymeric liquids in elongational flow with dissipation," J. Rheol. **48**, 591–598 (2004a).

Joshi, Y. M., and M. M. Denn, "Failure and Recovery of entangled polymer melts in elongational flow," in *Rheology Reviews 2004*, edited by K. Walters and D. Binding (British Society of Rheology, Abrystwyth, 2004b).

Kahvand, H., "Strain coupling effects in polymer rheology," Ph.D. dissertation, Illinois Institute Technology, Chicago, 1995.

Kremer, K., and G. S. Grest, "Dynamics of entangled linear polymer melts: A molecular dynamics simulation," J. Chem. Phys. **92**, 5057–5087 (1990).

Kushwaha, A., and E. S. G. Shaqfeh, "Slip-link simulations of entangled polymers in planar extensional flow: Disentanglement modified extension thinning," J. Rheol. **55**, 463–483 (2011).

Larson, R. G., *Constitutive Equations for Polymer Melts and Solutions* (Butterworth-Heinemann, Waltham, MA, 1988), p. 158.

Likhtman, A., "Single-chain slip-link model of entangled polymers: Simultaneous description of neutron spin-echo, rheology, and diffusion," Macromolecules **38**, 6128–6139 (2005).

Likhtman, A., S. K. Sukumaran, and J. Ramirez, "Linear viscoelasticity from molecular dynamics simulation of entangled polymers," Macromolecules **40**, 6748–6757 (2007).

Malkin, A. Ya., A. V. Semakov, and V. G. Kulichikhin, "Modeling macromolecular movement in polymer melts and its relation to nonlinear rheology," Rheol. Acta **50**, 485–489 (2011).

Marrucci, G., "Dynamics of entanglements: A nonlinear model consistent with the Cox-Merz rule," J. Non-Newtonian Fluid Mech. **62**, 279–289 (1996).

Marrucci, G., and G. Ianniruberto, "Interchain pressure effect in extensional flows of entangled polymer melts," Macromolecules **37**, 3934–3942 (2004).

Masubuchi, Y., G. Ianniruberto, F. Greco, and G. Marrucci, "Entanglement molecular weight and frequency response of sliplink networks," J. Chem. Phys. **119**, 6925–6930 (2003).

Masubuchi, Y., J. Ichi Takimoto, K. Koyama, G. Ianniruberto, G. Marrucci, and F. Greco, "Brownian simulations of a network of reptating primitive chains," J. Chem. Phys. **115**, 4387–4394 (2001).

McLeish, T. C. B., "Tube theory of entangled polymer dynamics," Adv. Phys. **51**, 1379–1527 (2002).

Mead, D. W., "The reptation model with chain stretching. I. Basic equations and general properties," Rheol. Acta **34**, 339–360 (1995a).

Mead, D. W., "The reptation model with chain stretching. II. Steady flow properties," Rheol. Acta **34**, 360–383 (1995b).

Mead, D. W., "Development of the 'binary interaction' theory for entangled polydisperse linear polymers," Rheol. Acta **46**, 369–395 (2007).

Mead, D. W., R. G. Larson, and M. Doi, "A molecular theory for fast flows of entangled polymers," Macromolecules **31**, 7895–7914 (1998).

Milner, S. T., T. C. B. McLeish, R. N. Young, A. Hakiki, and J. M. Johnson, "Dynamic dilution, constraint-release, and star-linear blends," Macromolecules **31**, 9345–9353 (1998).

Nair, D. M., and J. D. Schieber, "Linear viscoelastic predictions of a consistently unconstrained Brownian slip-link model," Macromolecules **39**, 3386–3397 (2006).

Neergaard, J., K. Park, D. C. Venerus, and J. D. Schieber, "Exponential shear flow of linear, entangled polymeric liquids," J. Rheol. **44**, 1043–1054 (2000).

Oberhauser, J. P., K. Pham, and L. G. Leal, "Rheo-optical studies of the response of entangled polymer solutions to step changes in shear rate," J. Rheol. **48**, 1229–1249 (2004).

Öttinger, H. C., "A thermodynamically admissible reptation model for fast flows of entangled polymers," J. Rheol. **43**, 1461–1493 (1999).

Pattamaprom, C., and R. G. Larson, "Constraint release effects in monodisperse and bidisperse polystyrenes in fast transient shearing flows," Macromolecules **34**, 5229–5237 (2001).

Pearson, D. S., E. A. Herbolzheimer, N. Grizzuti, and G. Marrucci, "Transient behavior of entangled polymers at high shear rates," J. Polym. Sci.: Phys. Ed. **29**, 1589–1597 (1991).

Rubinstein, M., "Discretized model of entangled-polymer dynamics," Phys. Rev. Lett. **59**, 1946–1949 (1987).

Rubinstein, M., and S. Panyukov, "Elasticity of polymer networks," Macromolecules **35**, 6670–6686 (2002).

Schieber, J. D., D. M. Nair, and T. Kitkrailard, "Comprehensive comparisons with nonlinear flow data of a consistently unconstrained Brownian slip-link model," J. Rheol. **51**, 1111–1141 (2007).

Simmons, J. M., "Dynamic modulus of polyisobutylene solutions in superposed steady shear," Rheol. Acta **7**, 184–188 (1968).

Somma, E., O. Valentino, G. Titomanlio, and G. Ianniruberto, "Parallel superposition in entangled polydisperse polymer melts: Experiment and theory," J. Rheol. **51**, 987–1005 (2007).

Struglinski, M. J., and W. W. Graessley, "Effects of polydispersity on the linear viscoelastic properties of entangled polymers. Part 3. Experimental observations on binary mixtures of linear and star polybutadienes," Macromolecules **21**, 783–789 (1988).

Tasaki, H., J.-I. Takimoto, and M. Doi, "Prediction of the rheological properties of polymers using a stochastic simulation," Comput. Phys. Commun. **142**, 136–139 (2001).

Tzoumanekas, C., and D. N. Theodorou, "From atomistic simulations to slip-link models of entangled polymer melts: Hierarchical strategies for the prediction of rheological properties," Curr. Opin. Solid State Mater. Sci. **10**, 61–72 (2006).

Van Kampen, N. G., *Stochastic Processes in Physics and Chemistry* (North-Holland, Amsterdam, 1992), pp. 373–374.

Venerus, D. C., and H. Kahvand, "Doi-Edwards evaluation in double step strain flows," J. Polym. Sci., Polym. Phys. Ed. **32**, 1531–1542 (1994).

Wagner, M. H., S. Kheirandish, and O. Hassager, "Quantitative prediction of transient and steady-state elongational viscosity of nearly monodisperse polystyrene melts," J. Rheol. **49**, 1317–1327 (2005).

Wagner, M. H., V. H. Rolon-Garrido, J. K. Nielsen, H. K. Rasmussen, and O. Hassager, "A constitutive analysis of transient and steady-state elongational viscosities of bidisperse polystyrene blends," J. Rheol. **52**, 67–86 (2008).

Wiest, J. M., "A differential constitutive equation for polymer melts," Rheol. Acta **28**, 4–12 (1989).

Yaoita, T., T. Isaki, Y. Masubuchi, H. Watanabe, G. Ianniruberto, F. Greco, and G. Marrucci, "Statics, linear, and nonlinear dynamics of entangled polystyrene melts simulated through the primitive chain network model," J. Chem. Phys. **128**, 154901 (2008).

Xu, F., M. M. Denn, and J. D. Schieber, "A full chain stochastic tube model for entangled melts and solutions of linear polymers," J. Rheol. **50**, 477–494 (2006).

Xu, F., M. M. Denn, and J. D. Schieber, "Stochastic chain simulation of wall slip in entangled melts," J. Rheol. **51**, 451–464 (2007).

Ye, X., R. G. Larson, C. Pattamaprom, and T. Sridhar, "Extensional properties of monodisperse and bidisperse polystyrene solutions," J. Rheol. **47**, 443–468 (2003).